EPJ Web of Conferences **262**, 01018 (2022) https://doi.org/10.1051/epjconf/202226201018
EXA2021

Antiproton-nuclei cross sections with Woods-Saxon potential at low energies

Andrea Bianconi[1,2], *Giovanni* Costantini[1,2], *Giulia* Gosta[1,2], *Marco* Leali[1,2], *Valerio* Mascagna[1,2], *Stefano* Migliorati[1,2,*], and *Luca* Venturelli[1,2]

[1]Dipartimento di Ingegneria dell'Informazione (DII), Università degli Studi di Brescia, Brescia, Italy
[2]INFN - Sezione di Pavia, Pavia, Italy

Abstract. The present knowledge of the antinucleons elastic scattering and annihilation processes in matter at low energies is limited to a few nuclei data in a small phase-space. Optical potential models are useful tools for modelling nuclear strong interaction of antinucleons with matter providing predictions at very low energies where data are missing. New calculations of elastic and annihilation cross sections for antiproton with nuclei using an optical potential of Woods-Saxon (WS) shape are presented. Preliminary predictions at low energies for carbon and calcium show clearly-measurable nuclear effects for nuclear elastic cross sections at large angles and momenta greater than 50 MeV/c. Some discrepancies in annihilation cross section comparing predictions and data are present using the same fitting parameters.

1 Introduction

During the 1980s and 1990s, experiments at Low Energy Antiproton Ring (LEAR) explored antinucleons annihilation and elastic scattering processes at low energy ($E < 50$ MeV) with different nuclei [1–16]. More recently, annihilation cross section with antiprotons of momentum $p = 100$ MeV/c (correponding to kinetic energy of $E = 5.3$ MeV) were measured by the ASACUSA collaboration [17–21] at the Antiproton Decelerator (AD) facility. In addition, other very low-energy measurements ($E = 125$ keV) were performed by the same collaboration on some nuclei, obtaining upper and lower limits of the values of annihilation cross sections [22]. The knowledge of the antinucleons-nucleus interaction at low energies is of interest for nuclear physics studies, in particular for the search of nuclear resonance and the determination of potential parameters. Futhermore, annihilation cross sections can also provide useful information about possible signals of antimatter presence in the Universe in the frame of some cosmological hypotheses [23, 24]. The knowledge of annihilation processes at low energies is also useful to study low-energy antiprotons from extra-atmospheric cosmic rays [25, 26] and also for medical physics applications [27–29]. Predictions at low energy can be used to design new experiments with enough sensitivity to study nuclear interaction effects and to observe other possible exotic processes.

In the present work, a six free-parameters Woods-Saxon (6pWS) optical potential has been chosen to model the strong interaction at low energies for the study of antiproton interaction with nuclei. With this optical potential, we are able to determine the parameters of the differential cross section for elastic scattering process of antiprotons with three nuclei of increasing mass: carbon-12 (^{12}C), calcium-40 (^{40}Ca) and lead-208 (^{208}Pb). We validate the model by comparing the annihilation cross sections, calculated with the obtained parameters, with the available data at low and intermediate momenta (p = 50–900 MeV/c). After this validation, we use the model to evaluate the elastic scattering differential cross sections at low momenta (with p = 15–100 MeV/c) considering in particular large angles (*i.e.* $\theta > 90°$).

The discussion is organized as follow. In Section 2, a brief review about optical potentials and partial wave expansion formalism is given; moreover, the choice of our model is presented and the fitting methods are briefly described. In Section 3, we present the main results of our analysis and a discussion about low-energy predictions of annihilation cross sections and on differential elastic scattering cross sections at large angles. In Section 4, a summary and possible future developments of the present analysis conclude the discussion.

2 Methods

To describe nuclear phenomena, a function for the nuclear strong potential generated by the target nucleus is defined. This potential depends on some parameters that describe its shape and on kinetics variables of both target and projectile. Strong potential of the system is usually modelled as a complex optical potential:

$$V_{opt}(r,k) = -[U(r,k) + iW(r,k)] \tag{1}$$

where r is the radial position with respect to the center of the (spherical) nucleus and $k = p/\hbar$ is the wave number of the projectile with momentum p in the lab frame. The

*e-mail: s.migliorati016@unibs.it

real part of the potential accounts for nuclear elastic scattering processes, while the imaginary part represents inelastic processes. These inelastic processes, at low energy, are dominated by annihilation and charge exchange. Other processes (*e.g.* knockout reactions) contribute in minor percentage to the reaction cross section. From now on we will refer to reaction cross sections at low energy as annihilation cross sections, also above the threshold for which the charge exchange start to contribute, *i.e.* $E \sim 5\,\mathrm{MeV}$.
The shape of the optical potential can vary, depending on the used model. In such models, it is important to describe appropriately the surface of the nucleus. In fact, if the potential shape is step-like (*e.g.* square-well) the annihilation cross section results underestimated [30]. A Woods-Saxon (WS) function is frequently used to accomplish the requirement of "smoothed" surface. The 2-parameter WS (2pWS) function is defined by:

$$F_{WS}(r \mid r_0, a_0) = \left[1 + \exp\left(\frac{r - r_0}{a_0}\right)\right]^{-1} \tag{2}$$

where r_0 is the nuclear radius, and a_0 is the diffuseness of the potential (the nuclear "surface thickness"). Therefore, the optical potential can be written as:

$$\begin{aligned} V_{opt}(r) = & -[U_0(k)\, F_{WS}(r \mid r_{0,U}, a_{0,U}) \\ & + iW_0(k)\, F_{WS}(r \mid r_{0,W}, a_{0,W})] \end{aligned} \tag{3}$$

where U_0 and W_0 are the strengths of the real and imaginary parts of the potential.

The optical potential is then used in a differential equation which describes the system under analysis. In this case, the system is a projectile particle which collides with a nucleus target. To describe low-energy particles, a non-relativistic Schrödinger equation is a good approximation. Therefore, the projectile-target system is described by the following equation:

$$\left(\frac{\hbar^2}{2\mu}\nabla^2 - V_C(r) - V_{opt}(r)\right)\psi(\mathbf{r}) = 0 \tag{4}$$

where V_C is the Coulomb potential of the projectile-target system:

$$V_C(r) = \begin{cases} \frac{Z_t Z_p e^2}{2R_C}\left(3 - \frac{r^2}{R_C^2}\right), & r \le R_C \\ \frac{Z_t Z_p e^2}{r}, & r > R_C. \end{cases} \tag{5}$$

Z_t and Z_p are respectively the target and projectile charge in unit of elementary charge, e (in the antiproton case $Z_p = -1$) and R_C is the Coulomb radius that we assume to be $R_C = 1.25\,A^{1/3}$ fm where A is the mass of the nucleus[1]. The equation is solved in partial-waves formalism, where the solution has the form:

$$\psi(r, \theta) \propto e^{ikz} + \frac{e^{ikr}}{r} f(\theta, k) \tag{6}$$

with f the scattering amplitude of the outgoing wave and θ the angle between the direction of the incoming wave (along the z-axis) and the direction of the outgoing wave. This scattering amplitude is the sum of contributions from many partial-waves with different angular momentum quantum number l. The general expression for f is:

$$f(\theta, k) = \frac{1}{2ik}\sum_{l=0}^{l_{max}} (2l+1)(\bar{S}_l - 1)P_l(\cos\theta) \tag{7}$$

where $\bar{S}_l$ is a function of l that contains the phase shift produced by the interaction under analysis. In principle, $l_{max} \to \infty$; however, for low energy projectiles and medium-light nuclei targets, only a limited number of partial-wave significantly contributes to the calculation. Considering both Coulomb and nuclear strong interactions acting in the processes, we define a total scattering amplitude:

$$f_{tot}(\theta, k) = f_C(\theta, k) + f_N(\theta, k) \tag{8}$$

$$f_C(\theta, k) = \frac{1}{2ik}\sum_{l=0}^{l_{max}} (2l+1)(e^{2i\sigma_l} - 1)P_l(\cos\theta) \tag{9}$$

$$f_N(\theta, k) = \frac{1}{2ik}\sum_{l=0}^{l_{max}} (2l+1)e^{2i\sigma_l}(S_l - 1)P_l(\cos\theta). \tag{10}$$

f_C is the Coulomb-only scattering amplitude, assuming a point-like target-charge; f_N is the nuclear scattering amplitude, which include the influence of the Coulomb interaction of the nucleus; $\sigma_l = \arg[\Gamma(1 + l + i\eta)]$ is the Coulomb phase shift, where Γ is the Euler gamma function, $\eta = Z_t e^2 \mu/\hbar p$ is the Sommerfeld parameter, with μ the reduced mass of the projectile-target system. S_l is the nuclear factor which contains quantitative information about the interaction. The cross sections relate to f_{tot} and S_l by:

$$\begin{aligned} \frac{d\sigma_{el}}{d\Omega} &= |f_{tot}(\theta)|^2 = \\ &\frac{1}{4k^2}\left|\sum_{l=0}^{l_{max}} (2l+1)(e^{2i\sigma_l}S_l - 1)P_l(\cos\theta)\right|^2 \end{aligned} \tag{11}$$

$$\sigma_{el}(k) = \frac{\pi}{k^2}\sum_{l=0}^{l_{max}} (2l+1)\left|e^{2i\sigma_l}S_l - 1\right|^2 \tag{12}$$

$$\sigma_{an}(k) = \frac{\pi}{k^2}\sum_{l=0}^{l_{max}} (2l+1)(1 - |S_l|^2) \tag{13}$$

where $d\sigma_{el}/d\Omega$ is the differential elastic cross section and σ_{an} is the annihilation cross section. The function f_N is calculated using a Fortran code derived from `THREEDEE` by Chant and Roos [31], which solves the Schrödinger equation in presence of the Coulomb potential and the 6pWS optical potential to model the strong interaction. The code calculations are up to $l = l_{max} = 120$. The differential elastic cross section and the other quantities are then computed for a specific momentum and angle.

Using this code, we fit to differential nuclear elastic cross section data minimizing a standard-χ^2. The parameters to be calculated are the six ones of the optical potential (real and imaginary parts) of Eqn 3. Standard algorithms of `ROOT` packages (*e.g.*, `TMinuit` library) [32] were used

[1] A is expressed in atomic mass unit (amu).

to find the minimum of the χ^2. We also estimate the 95% Confidence Interval (CI) band of the best fit lines, using:

$$CI_{95\%} = t_{NDF-1,\,0.95}\,\delta_{X,th} \tag{14}$$

where NDF are the number of degrees of freedom – number of data used for the fit minus the number of free-parameters –, t is the t-Student quantile and $\delta_{X,th}$ is the error estimation of the theoretical differential cross-section $X^{(th)}$ via error propagation.

3 Results and discussion

We fit our model to differential elastic cross section data of three different nuclei with increasing mass: ^{12}C, ^{40}Ca and ^{208}Pb. These data are from Garreta *et al.* (PS184 experiment at LEAR) [33] and Janouin *et al.* [34]. The results of the fitting procedure can be found in Table 1.

We have assumed $U_0(k) = U_0$ and $W_0(k) = W_0$. Also, the function $F_{WS}(r)$ is reparametrized as:

$$F_{WS}(r) = \left[1 + \exp\left(\frac{r - r_{0,x}A^{1/3}}{a_{0,x}}\right)\right]^{-1} \tag{15}$$

where $x = U, W$.

Table 1. Best-fitting parameters of the 6pWS optical potential. Data for fitting are from Ref. [33, 34]. Antiproton momenta for the given targets are 608 MeV/c (^{12}C and ^{40}Ca) and 305 MeV/c (^{208}Pb). Errors are estimated automatically by ROOT algorithms. The reduced-χ^2 of the fit, defined as $\tilde{\chi}^2 = \chi^2/NDF$, is also reported.

Target	^{12}C	^{40}Ca	^{208}Pb
U_0(MeV)	79.2 ± 0.7	28 ± 2	4.0 ± 0.6
W_0(MeV)	50.8 ± 2	22 ± 3	9 ± 1
$r_{0,U}$(fm)	1.066 ± 0.002	1.34 ± 0.02	1.40 ± 0.04
$r_{0,W}$(fm)	1.26 ± 0.02	1.35 ± 0.02	1.40 ± 0.02
$a_{0,U}$(fm)	0.361 ± 0.004	0.38 ± 0.02	0.30 ± 0.05
$a_{0,W}$(fm)	0.465 ± 0.007	0.55 ± 0.03	0.50 ± 0.02
$\tilde{\chi}^2$	58.9/42 ≈ 1.4	95.6/38 ≈ 2.5	78/13 ≈ 6.0

From Table 1, a decreasing in values of U_0 and W_0 with the increasing of A can be noticed. However, it is very difficult to find a precise relation between the two quantities with such poor analysis. For ^{40}Ca and ^{208}Pb, $r_{0,U} = r_{0,W}$, a common assumption in this kind of model (see for example Ref. [34]); on the contrary, for ^{12}C this is not valid ($r_{0,U} < r_{0,W}$). We also let $a_{0,U}$ and $a_{0,W}$ as free-parameters, obtaining for all nuclei $a_{0,U} > a_{0,W}$. The values of $a_{0,x}$ are quite stable for increasing A, while $r_{0,x}$ slightly increase with A. Concerning the real and imaginary strengths of the potential, with exception of the ^{208}Pb, we observe $U_0 > W_0$ in ^{12}C and ^{40}Ca. The interpretation of these results at the moment is not completely clear and requires a deeper and more complete analysis.
We have also to clarify that important correlation values are found for some parameters pairs.

In Figures 1, 2 and 3, we compare the best fit line - together with the 95% CI band estimation - with the data used for fitting. The agreement is satisfactory for

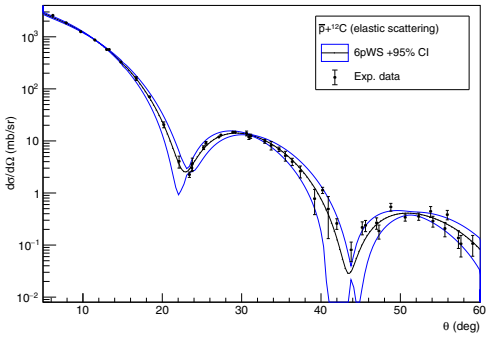

Figure 1. ^{12}C data at $p = 608$ MeV/c and best fit line with 6pWS with the 95% confidence interval. The reported parameters are from Table 1, while data are from Ref. [33].

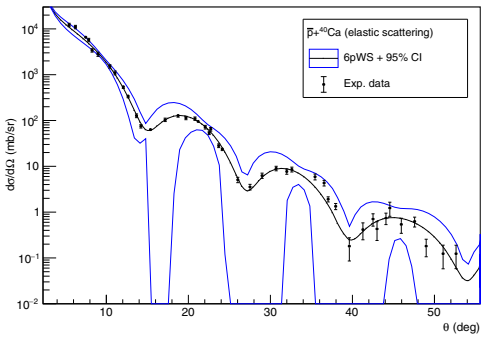

Figure 2. ^{40}Ca data at $p = 608$ MeV/c and best fit line with 6pWS with the 95% confidence interval. The reported parameters are from Table 1, while data are from Ref. [33].

^{12}C and ^{40}Ca targets. Some discrepancies are present in the ^{208}Pb case at small angles. Furthermore, the fitting procedure gives different problems with the latter target, since the algorithms have difficulty to converge to a unique solution. Therefore, from now on, we will not consider ^{208}Pb in our analysis and we will reconsider it in the future with an improved fitting procedure.

The 6pWS model is then applied to the annihilation process for ^{12}C and ^{40}Ca. We assume that the same parameters determined from elastic scattering process are valid also in this case. The annihilation cross sections in dependence of the antiproton momentum p is calculated using Eqn. 13 with the parameters in Table 1. The results of such calculations for p from 50 MeV/c to 1000 MeV/c can be found in Figures 4 and 5. For the ^{12}C case, we compare the results with data from different measurement: the 100 MeV/c by the ASACUSA collaboration [18] and the measurements by Nakamura *et al.* [35] between 450 MeV/c and 900 MeV/c. In addition, a compar-

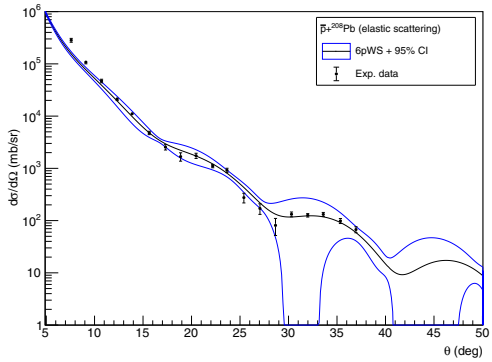

Figure 3. ^{208}Pb data at $p = 305\,\mathrm{MeV/c}$ and best fit line with 6pWS with the 95% confidence interval. The reported parameters are from Table 1, while data are from Ref. [33].

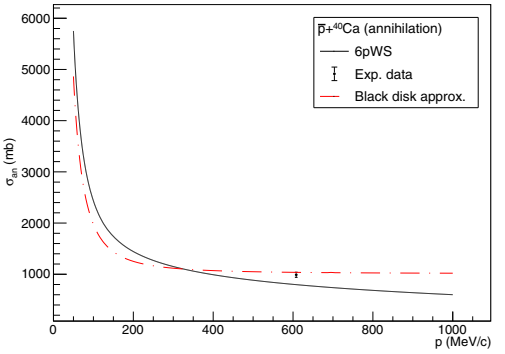

Figure 5. ^{40}Ca annihilation cross section calculation and data. The parameters are from Table 1.

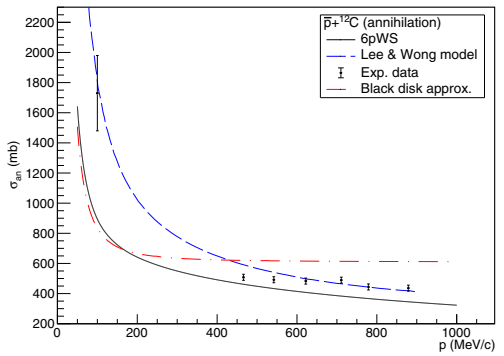

Figure 4. ^{12}C annihilation cross section calculations and data. The parameters are from Table 1.

ison with two different models is done. The blue dashed line is the fitting result of the optical potential proposed by Lee and Wong where they include the dependence of momentum for the real strength $U_0(k)$ [36]. The red dot-dashed line is the "black disk" approximation by Batty *et al.* [37] considering the low-energy regime of the antiproton with the Coulomb focusing due to the charge of the nucleus:

$$\sigma_{an}(k) \approx \pi R^2 \left(1 + \frac{2mZ_t e^2}{\hbar^2 k_{cm} k_{lab} R}\right) \tag{16}$$

where $R = (1.840 + 1.120\,A^{1/3})$ fm and m is the antiproton mass. $k_{cm} = p_{cm}/\hbar$ is the center-of-mass frame wave number[2] and $k_{lab} = p/\hbar$ is the lab-frame wave number.

[2]The center-of-mass momentum p_{cm} can be calculated using the relativistic formula:

$$p_{cm} = \frac{1}{2\sqrt{s}} \left\{\left[s - (m_{\bar{p}} - m_A)^2\right]\left[s - (m_{\bar{p}} + m_A)^2\right]\right\}^{\frac{1}{2}}$$

where $s = (p^{\mu}_{\bar{p}} + p^{\mu}_{A})^2$ (the first Mandelstam variable), and $m_{\bar{p}}$, m_A are the antiproton and nucleus masses.

The 6pWS model results are in agreement with the available carbon-12 data within 2-3 standard-deviation. This is quite satisfying especially considering that our parameters are determined from the fitting to elastic scattering data and not to annihilation data. The behaviour of the curve and the distance from experimental data are quite good, considering the assumptions.

The ^{40}Ca case is more difficult to analyse, due to the scarcity of annihilation cross sections data. The only one shown in Fig. 5 is from Garreta *et al.* [33], at $p = 608\,\mathrm{MeV/c}$. The single datum of ^{40}Ca is one standard-deviation within the black disk approximation and about 4 standard-deviations within our 6pWS prediction.

Both in the ^{12}C and ^{40}Ca analyses, our predictions underestimate the experimental values. Nevertheless, the calculated values are in quite good agreement with available data, reproducing also quite well the behaviour in dependence of the momentum. Therefore, our obtained parameters are enough reliable to use them to make predictions in low-energy regime for differential elastic cross sections.

In Fig.s 6 and 7 for momenta greater than $50\,\mathrm{MeV/c}$ the Coulomb (dashed lines) and total contribution (solid lines) are clearly distinguishable at large angles. On the contrary, for $p < 50\,\mathrm{MeV/c}$ it is difficult to clearly see in a measurement the nuclear contributions from the Rutherford ones. These observations are valid for both ^{12}C and ^{40}Ca targets, as can be seen in the figures mentioned above.

The 6pWS model, with the parameters obtained by the fitting, therefore suggests the possibility to see nuclear effects in elastic scattering measurement for $p > 50\,\mathrm{MeV/c}$ and at large angles. Under this momentum (and for angles smaller than 90°), it seems to be very difficult to measure such contributions. Similar results for the angular distribution at low energy were found by Protasov *et al.* [38] for the ^{12}C case using a different parametrization of the optical potential.

As shown in Fig. 8, in their case (solid blue line) nuclear effects at $50\,\mathrm{MeV/c}$ are more accentuated than in our

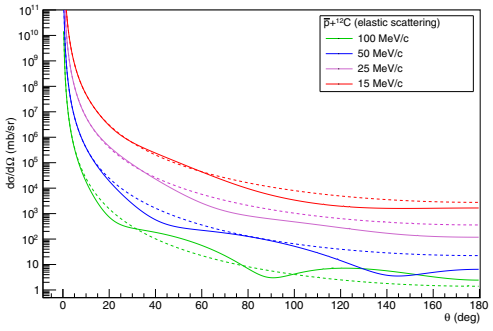

Figure 6. ^{12}C differential elastic cross section in low momentum regime, from 15 MeV/c to 100 MeV/c. In dashed line the correspondent Coulomb cross sections is shown. The parameters are taken from Table 1.

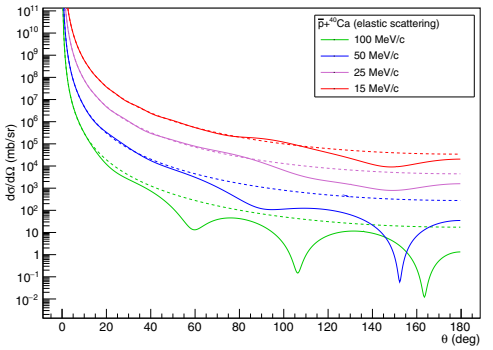

Figure 7. ^{40}Ca differential elastic cross section in low momentum regime, from 15 MeV/c to 100 MeV/c. In dashed line the correspondent Coulomb cross sections is shown. The parameters are taken from Table 1.

calculations (solid black line), resulting in a lower limit estimation for measurements ($p > 20$ MeV/c). This discrepancy between our model and theirs is complicate to be understood. One possible explanation could be the different parametrization of the potential and the different kind of parameters used. However, both the behaviour of the curve and the position of the minimum around 145 MeV/c are very similar in the two predictions.

4 Summary and future developments

A six free-parameter Woods-Saxon (6pWS) optical potential is fitted to differential elastic scattering cross section data available for antiproton projectiles on medium-light (^{12}C, ^{40}Ca) and heavy (^{208}Pb) nuclei at intermediate energy. We validate these results comparing the annihilation cross section measurements with the calculations of our model, confirming a satisfying agreement with available data. The agreement is quite good (2-4 experimental errors), considering the free-parameters of the model are obtained from different types of data, some discrepancies are present. Then, we use the obtained parameters to predict the differential elastic cross sections at low momenta ($p < 100$ MeV/c), focusing on large-angles behaviour. Nuclear effects seems to be observable for momentum greater than 50 MeV/c, while under this value Coulomb contribution begins to hide the nuclear contribution. In our knowledge, no such predictions at low energy exists in literature (a part from the very recent work by Protasov *et al.* [38]) and also measurements of this kind do not exist, in particular at large angles.

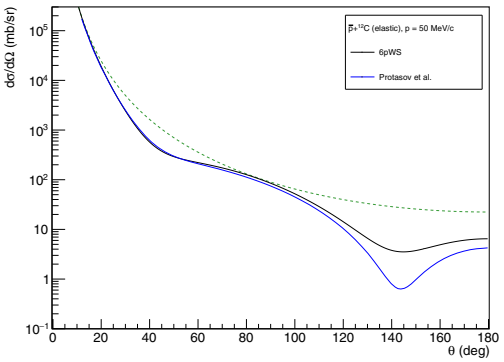

Figure 8. ^{12}C differential elastic cross section at $p = 50$ MeV/c. In solid black line, our model; in solid blue line the calculation by Protasov *et al.* [39] The dashed green line is the Rutherford scattering cross section.

Some improvements are necessary to our model. A Lee and Wong approach, introducing dependences on antiproton momentum, is a possible path to follow. Moreover, some other terms can be introduced in the potential, *e.g.* an absorption surface term proportional to $dF_{WS}(r)/dr$. Also, we have to consider other possible parametrizations of the optical potential more suitable for our purpose, like the one proposed by Batty, Friedman and Gal [40]. Other future developments of this analysis can include better evaluation of uncertainties and correlations of the parameters, and the use of more efficient algorithms. These improvements on antiproton analysis are useful to design antiproton experiments at low energy, *e.g.* at ELENA (Extra Low ENergy Antiproton) ring [41] at AD and at FLAIR (Facility for Low-energy Antiproton and Ion Research) at GSI [42, 43]. Finally, a fundamental step will be to include the present calculations and analysis for antineutrons. The extension of our analysis to antineutrons scattering can be useful to dispel some incongruities highlighted by Friedman [44]. Moreover, the determination of the scattering length of the antineutron is a necessary step to design experiments (*e.g.*, for neutron-antineutron oscillation [38, 39, 45]). Further measurements of annihilation – in particular between 100 and 450 MeV/c – and nuclear elastic scattering cross sections at low energies ($p > 50$ MeV/c) and large angles ($\theta > 90°$)

could be useful to improve phenomenological models for nuclear strong interactions. Facilities which could provide in future such experimental conditions are ELENA and FLAIR.

References

[1] R. Bizzarri, P. Guidoni, F. Marcelja, F. Marzano, E. Castelli, M. Sessa, Il Nuovo Cimento A (1965-1970) **22**, 225 (1974)

[2] B. Gunderson, J. Learned, J. Mapp, D. Reeder, Physical Review D **23**, 587 (1981)

[3] F. Balestra, Y.A. Batusov, G. Bendiscioli, M. Bussa, L. Busso, I. Falomkin, L. Ferrero, V. Filippini, G. Fumagalli, G. Gervino et al., Physics Letters B **149**, 69 (1984)

[4] F. Balestra, S. Bossolasco, M.P. Bussa, L. Bussa, L. Ferrero, D. Panzieri, G. Piragino, F. Tosello, C. Guaraldo, A. Maggiora et al., Physics Letters B **165**, 265 (1985)

[5] M. Agnello, F. Iazzi, B. Minetti, L. Cugusi, M. Macciotta, S. Marcello, A. Masoni, G. Puddu, A. Raimondi, S. Serci et al., EPL (Europhysics Letters) **7**, 13 (1988)

[6] F. Balestra, R. Barbieri, Y.A. Batusov, G. Bendiscioli, S. Bossolasco, F. Breivik, M.P. Bussa, L. Busso, C. Guaraldo, I. Falomkin et al., Physics Letters B **230**, 36 (1989)

[7] W. Brückner, B. Cujec, H. Döbbeling, K. Dworschak, F. Güttner, H. Kneis, S. Majewski, M. Nomachi, S. Paul, B. Povh et al., Zeitschrift für Physik A Atomic Nuclei **335**, 217 (1990)

[8] V. Ableev, A. Adamo, M. Agnello, F. Balestra, G. Belli, G. Bendiscioli, A. Bertin, P. Boccaccio, G. Bonazzola, E. Botta et al., Il Nuovo Cimento A (1965-1970) **107**, 943 (1994)

[9] C. Barbina, A. Ahmidouch, R. Birsa, F. Bradamante, A. Bressan, S. Dalla Torre-Colautti, M. Giorgi, R. Hess, F. Iazzi, R. Kunne et al., Nuclear Physics A **612**, 346 (1997)

[10] A. Benedettini, A. Bertin, M. Bruschi, M. Capponi, A. Collamati, I. D'Antone, S. De Castro, R. Dona, A. Ferretti, D. Galli et al., Nuclear Physics B-Proceedings Supplements **56**, 58 (1997)

[11] A. Zenoni, A. Bianconi, F. Bocci, G. Bonomi, M. Corradini, A. Donzella, E.L. Rizzini, L. Venturelli, A. Bertin, M. Bruschi et al., Physics Letters B **461**, 405 (1999)

[12] A. Zenoni, A. Bianconi, G. Bonomi, M. Corradini, A. Donzella, E.L. Rizzini, L. Venturelli, A. Bertin, M. Bruschi, M. Capponi et al., Physics Letters B **461**, 413 (1999)

[13] A. Bianconi, G. Bonomi, M. Bussa, E.L. Rizzini, L. Venturelli, A. Zenoni, G. Pontecorvo, C. Guaraldo, F. Balestra, L. Busso et al., Physics Letters B **481**, 194 (2000)

[14] A. Bianconi, G. Bonomi, M. Bussa, E.L. Rizzini, L. Venturelli, A. Zenoni, G. Pontecorvo, C. Guaraldo, F. Balestra, L. Busso et al., Physics Letters B **492**, 254 (2000)

[15] F. Iazzi, A. Feliciello, M. Agnello, M. Astrua, E. Botta, T. Bressani, D. Calvo, S. Costa, F. D'Isep, A. Filippi et al., Physics Letters B **475**, 378 (2000)

[16] M. Astrua, E. Botta, T. Bressani, D. Calvo, C. Casalegno, A. Feliciello, A. Filippi, S. Marcello, M. Agnello, F. Iazzi, Nuclear Physics A **697**, 209 (2002)

[17] A. Bianconi, M. Corradini, M. Hori, M. Leali, E.L. Rizzini, V. Mascagna, A. Mozzanica, M. Prest, E. Vallazza, L. Venturelli et al., Physics Letters B **704**, 461 (2011)

[18] H. Aghai-Khozani, A. Bianconi, M. Corradini, R. Hayano, M. Hori, M. Leali, E. Lodi Rizzini, V. Mascagna, Y. Murakami, M. Prest et al., Nuclear Physics A **970**, 366 (2018)

[19] M. Corradini, R. Hayano, M. Hori, M. Leali, E. Lodi Rizzini, V. Mascagna, A. Mozzanica, M. Prest, K. Todoroki, E. Vallazza et al., Nuclear Instruments and Methods in Physics Research Section A: Accelerators, Spectrometers, Detectors and Associated Equipment **711**, 12 (2013)

[20] K. Todoroki, D. Barna, R. Hayano, H. Aghai-Khozani, A. SÃ³tÃ©r, M. Corradini, M. Leali, E. Lodi-Rizzini, V. Mascagna, L. Venturelli et al., Nuclear Instruments and Methods in Physics Research Section A: Accelerators, Spectrometers, Detectors and Associated Equipment **835**, 110 (2016)

[21] M. Corradini, M. Leali, E.L. Rizzini, V. Mascagna, M. Prest, E. Vallazza, L. Venturelli, Hyperfine Interactions **233**, 53 (2015)

[22] H. Aghai-Khozani, D. Barna, M. Corradini, D. De Salvador, R. Hayano, M. Hori, M. Leali, E. Lodi-Rizzini, V. Mascagna, M. Prest et al., Nuclear Physics A **1009**, 122170 (2021)

[23] A.G. Cohen, A.D. Rújula, S.L. Glashow, **495**, 539 (1998)

[24] H. Kurki-Suonio, E. Sihvola, Phys. Rev. Lett. **84**, 3756 (2000)

[25] K. Abe, H. Fuke, S. Haino, T. Hams, A. Itazaki, K. Kim, T. Kumazawa, M. Lee, Y. Makida, S. Matsuda et al., Physics Letters B **670**, 103 (2008)

[26] T. Aramaki, S. Boggs, P. von Doetinchem, H. Fuke, C. Hailey, S. Mognet, R. Ong, K. Perez, J. Zweerink, Astroparticle Physics **59**, 12 (2014)

[27] L. Gray, T.E. Kalogeropoulos, Radiation Research **97**, 246 (1984)

[28] M.H. Holzscheiter, N. Bassler, N. Agazaryan, G. Beyer, E. Blackmore, J.J. DeMarco, M. Doser, R.E. Durand, O. Hartley, K.S. Iwamoto et al., Radiotherapy and Oncology **81**, 233 (2006)

[29] N. Bassler, M.H. Holzscheiter, H. Knudsen, AIP Conference Proceedings **796**, 423 (2005)

[30] H. Feshbach, Annual Review of Nuclear Science **8**, 49 (1958)

[31] N.S. Chant, P.G. Roos (1998), (unpublished)

[32] R. Brun, F. Rademakers, P. Canal, A. Naumann, O. Couet, L. Moneta, V. Vassilev, S. Linev, D. Piparo, G. GANIS et al., *root-project/root: v6.18/02* (2019), https://doi.org/10.5281/zenodo.3895860

[33] D. Garreta, P. Birien, G. Bruge, A. Chaumeaux, D. Drake, S. Janouin, D. Legrand, M. Lemaire, B. Mayer, J. Pain et al., Physics Letters B **149**, 64 (1984)

[34] S. Janouin, M.C. Lemaire, D. Garreta, P. Birien, G. Bruge, D. Drake, D. Legrand, B. Mayer, J. Pain, J. Peng et al., Nuclear Physics A **451**, 541 (1986)

[35] K. Nakamura, J. Chiba, T. Fujii, H. Iwasaki, T. Kageyama, S. Kuribayashi, T. Sumiyoshi, T. Takeda, H. Ikeda, Y. Takada, Phys. Rev. Lett. **52**, 731 (1984)

[36] T.G. Lee, C.Y. Wong, Phys. Rev. C **97**, 054617 (2018)

[37] C. Batty, E. Friedman, A. Gal, Nuclear Physics A **689**, 721 (2001)

[38] K.V. Protasov, V. Gudkov, E.A. Kupriyanova, V.V. Nesvizhevsky, W.M. Snow, A.Y. Voronin, Phys. Rev. D **102**, 075025 (2020)

[39] V.V. Nesvizhevsky, V. Gudkov, K.V. Protasov, W.M. Snow, A.Y. Voronin, Phys. Rev. Lett. **122**, 221802 (2019)

[40] C. Batty, E. Friedman, A. Gal, Physics Reports **287**, 385 (1997)

[41] V. Chohan, C. Alanzeau, M. Angoletta, J. Baillie, D. Barna, W. Bartmann, P. Belochitskii, J. Borburgh, H. Breuker, F. Butin et al., *Extra Low ENergy Antiproton (ELENA) ring and its Transfer Lines: Design Report* (2014), ISBN 9789290834007

[42] E. Widmann, Physica Scripta **2015**, 014074 (2015)

[43] C.P. Welsch, A. Papash, O. Gorda, J. Harasimowicz, O. Karamyshev, G. Karamysheva, D. Newton, M. Panniello, M. Putignano, M. Siggel-King et al., Hyperfine Interactions **213**, 205 (2012)

[44] E. Friedman, Nuclear Physics A **925**, 141 (2014)

[45] J.L. Barrow, A.S. Botvina, E.S. Golubeva, J.M. Richard, *A new model of intranuclear neutron-antineutron transformations in* ${}^{16}_{8}O$ (2021), arXiv:2111.10478[hep-ex]